Bulk and surface thermal stability of ultra nanocrystalline diamond films with 10-30 nm grain size prepared by chemical vapor deposition

Bulk and surface thermal stability of ultra nanocrystalline diamond films with 10–30 nm grain size prepared by chemical vapor deposition

Sh. Michaelson,[1] A. Stacey,[2] J. Orwa,[2] A. Cimmino,[2] S. Prawer,[2] B. C. C. Cowie,[3] O. A. Williams,[4] D. M. Gruen,[5] and A. Hoffman[1,a)]
[1]*Schulich Faculty of Chemistry, Technion, Israel Institute of Technology, Haifa 32000, Israel*
[2]*School of Physics, The Melbourne University, Victoria 3010, Australia*
[3]*Australian Synchrotron, 800 Blackburn Road, Clayton, Victoria 3168, Australia*
[4]*Institut für Angewandte Festkörperphysik, Fraunhofer Gesellschaft, 79108 Freiburg, Germany*
[5]*Materials Science Division, Argonne National Laboratory, Illinois 60439, USA*

(Received 11 November 2009; accepted 14 February 2010; published online 6 May 2010)

The thermal stability of nanocrystalline diamond films with 10–30 nm grain size deposited by microwave enhanced chemical vapor deposition on silicon substrate was investigated as a function of annealing temperature up to 1200 °C. The thermal stability of the surface-upper atomic layers was studied with near edge x-ray absorption fine structure (NEXAFS) spectroscopy recorded in the partial electron yield mode. This technique indicated substantial thermally induced graphitization of the film within a close proximity to the surface. While in the bulk region of the film no graphitization was observed with either Raman spectroscopy or NEXAFS spectroscopy recorded in total electron yield mode, even after annealing to 1200 °C. Raman spectroscopy did detect the complete disappearance of transpolyacetylene (t-PA)-like ν_1 and ν_3 modes following annealing at 1000 °C. Secondary ion mass spectroscopy, applied to investigate this relative decrease in hydrogen atom concentration detected only a ~30% decrease in the bulk content of hydrogen atoms. This enhanced stability of sp^3 hybridized atoms within the bulk region with respect to graphitization is discussed in terms of carbon bond rearrangement due to the thermal decomposition of t-PA-like fragments. © *2010 American Institute of Physics*. [doi:10.1063/1.3359714]

I. INTRODUCTION

While macroscopic graphite is more stable than macroscopic diamond, with a very high (~7 eV/atom) activation energy for phase transition,[1] the opposite is true for nanometer sized carbon grains.[2] Graphitization mechanism of diamond and the preferential energetic stability of nanodiamond crystallites over graphitic particles of the same size has been the subject of rigorous research in the past decades.[2–11] The size, surface termination, and intergranular phase and chemical composition of the diamond crystallites affect the physical and electronic film properties, including the dielectric constant,[12,13] electron and field emission[14,15] and tribological properties,[16] etc. Elevated temperatures were also found to improve the field emission,[17] thermionic emission,[18] and secondary electron emission properties.[19] In nearly all electron emission cases, the surface of the film must be hydrogen passivated to induce negative electron affinity[20] and significantly enhance the electron emission yield.

Most experimental and theoretical works[2–11] studying the thermal stability of nanodiamond films have dealt with detonation nanodiamond,[21] while little has been done on chemically vapor deposited (CVD) films.[22–26] Considering the differences in intergrain composition and adhesion forces between these films, one may expect different thermal behavior especially for elevated temperatures. One of the most fascinating differences is the presence of hydrogen atoms, which are trapped in significant proportions within the CVD films. Hydrogen's high mobility and bonding may release accumulated stress in carbon layers,[27–29] as well as in other materials.[30] It was shown previously,[26,31–40] that polycrystalline CVD diamond film deposited in a hydrogen containing atmosphere (even from an H deficient/Ar rich gas phase with ~1% H_2) contains up to a few at. % of hydrogen atoms. The concentration of hydrogen correlates inversely[34,36–40] with the diamond grain size, reaching ~20 at. % for 5 nm diamond crystallites.[24] Our vibrational spectroscopy studies showed that these H atoms are bonded both to sp^2 and sp^3 hybridized carbon,[38,40] with most of the trapped hydrogen positioned at diamond grain boundaries as well as on the crystallite surfaces within the film. Therefore the role of hydrogen on the thermal stability of diamond nanocrystallite films must be considered. From a practical experimental point of view the thermal stability of different diamond films, especially in the nanocrystalline size regime, seems to be a very important issue. In nearly all cases diamond film deposition and surface characterization are carried out in different experimental chambers, causing the majority of films to be exposed to ambient conditions during sample transfer. *In situ* vacuum annealing procedures of at least 500 °C are a very simple way to remove ambient contamination from diamond surfaces, thus removing contaminant hydrocarbon and exposing hydrogen directly bonded to the diamond matrix of interest.[41] However in order to remove all the contaminants from the diamond surface, annealing must be performed at temperatures of 1000 °C or above.[42] This raises questions about surface reconstruction, hydrogen desorption induced

a)Author to whom correspondence should be addressed. Electronic mail: choffman@tx.technion.ac.il.

defects, and the degree of diamond graphitization of different diamond films following thermal annealing.

In the present work we study and compare the effect of thermal annealing, up to 1200 °C, on the bulk and surface of CVD deposited nanodiamond films. Analysis techniques include Raman spectroscopy for bulk analysis, while near-edge x-ray absorption fine structure (NEXAFS) can be utilized to independently analyze both bulk and surface regions. NEXAFS spectroscopy can be recorded by measuring both the bulk sensitive total electron yield (TEY) as well as the surface sensitive partial electron yield (PEY) from the sample. When recorded as a function of the photon excitation energy, exciting from the C(1s) core level, it has been shown to be a powerful probe of the diamond electronic structure.[43–46] Unlike Raman spectroscopy, NEXAFS has a similar cross section for different carbon allotropes and it is sensitive to local chemical bonding, which enables analysis of nanosized carbon materials.[47,48]

II. EXPERIMENTAL

Nanodiamond films were deposited with a 2.45 GHz microwave plasma enhanced chemical vapor deposition reactor. The Si substrate temperature was maintained at 800 °C along with a microwave power of 1200 W and total gas pressure of 200 Torr. Prior to deposition the silicon substrates were seeded mechanically in solution with diamond powder. The gas mixture composition was 1.4% CH_4, 1% H_2, and 97.6% Ar and final film thickness is ~2 μm. Under these deposition conditions the estimated growth rate is 2.7 μm/h with diamond grain sizes of 10–30 nm.[49,50]

The scanning probe microscopy measurements were performed in a JEOL SPM system at 10^{-6} Torr.[51] The samples were scanned with a conductive tip (heavily B-doped Si, coated with WC) in contact mode with controlled loading. The imaging scan was obtained by applying a positive bias of 8 V, while recording the tip-sample current. A silver contact was made directly to the diamond film, such that the bias was applied between the tip and the diamond film. Current images were obtained by plotting the measured current at a constant bias.

The NEXAFS measurements were conducted at the Australian synchrotron using an elliptically polarized undulator capable of providing photons in the energy range between 90 and 2000 eV.[52] The NEXAFS spectra were measured using a vacuum system consisting of four interconnected chambers: (i) a load lock with heating facilities, (ii) a preparation chamber, (iii) a central chamber used for sample transfer and storage, and (iv) a chamber dedicated to the NEXAFS measurements and connected to the beam line, equipped with an hemispherical analyzer, retarding field analyzer, and fluorescence yield device. The base pressure of the vacuum chamber where the NEXAFS measurements were conducted was better than 2×10^{-10} Torr.

The NEXAFS measurements were carried out in the 280–310 eV photon energy range in the PEY and TEY modes. The PEY measurements were carried out by recording the intensity of secondary electrons above 200 eV using a retarding field analyzer as a function of incident photon energy. The TEY was carried out by measuring the sample current as a function of photon energy. The TEY and PEY spectra were normalized to a similar spectra measured for a sputtered cleaned gold sample to cancel any contributions originating from carbon impurities present in the beam line which may contribute to changes in the photon intensity. The measurements were carried out by increasing the photon energies in steps of 0.05 eV. The energy scale of all spectra was fixed to the bulk second band-gap of diamond at 302.4 eV.

SIMS analysis was carried out in dynamic mode in a Cameca IMS4f ion microscope. The samples were irradiated by 14.5 keV Cs+ ion beam. The sampling area was about 64 μm^2. The basic chamber pressure was 8×10^{-10} Torr, while the ion current was about 1×10^{-8} A.

The Raman measurements were carried out using a Renishaw Raman microscope system and an incident light source of 514.5 nm. An incident laser power of 3 mW and $\times100$ objective were used in these measurements.

The thermal annealing system consisted of a large bell-jar type, diffusion pumped, vacuum chamber containing a graphite crucible sample holder directly heated by a tungsten filament. The temperature was recorded with both a thermocouple in contact with the graphite crucible and an optical pyrometer. Sample annealing up to 1200 °C was performed at pressure of 5×10^{-6} Torr (during heating) for 30 min. The annealing experiments for each temperature were carried out on different diamond film pieces from the same wafer.

III. RESULTS AND DISCUSSION

In the present discussion we contrast the surface and bulk stability of nanocrystalline diamond films and compare them with submicron and single crystal diamond. In Sec. III A the bulk thermal stability is studied with Raman and NEXAFS spectroscopies (the latter recorded in bulk sensitive mode), while the SIMS technique is applied to study the relative decrease in hydrogen atom concentration following 1000 °C annealing. In Sec. III B, the nanodiamond surface stability is studied with NEXAFS spectroscopy using PEY (surface sensitive mode). In Sec. III C we suggest a possible explanation for the enhanced stability of CVD nanodiamond bulk versus its surface region.

A. Nanodiamond bulk thermal stability study

First, we refer to the NEXAFS TEY results recorded in bulk sensitive mode (see Sec. II), shown in Fig. 1. We estimate that NEXAFS measured in the TEY mode is sensitive down to the 50–100 Å near surface region. Figure 1(a) shows the spectra of the nanodiamond film as-deposited and after annealing at 800 and 1000 °C. A single crystal (type IIA) sample which underwent 1000 °C treatment and an as-deposited polycrystalline diamond film with submicron grain size are included for comparison.

The well defined single crystalline diamond spectrum (upper line) is dominated by a sharp exciton peak at 289.3 eV and a broad dip fixed at 302.4 eV, which is associated with the second absolute band gap of diamond. A zoom of the pre-edge region is shown in Fig. 1(b). The peak at ~285 eV, which is due to the C(1s) $\rightarrow \pi^*$ resonance, can be

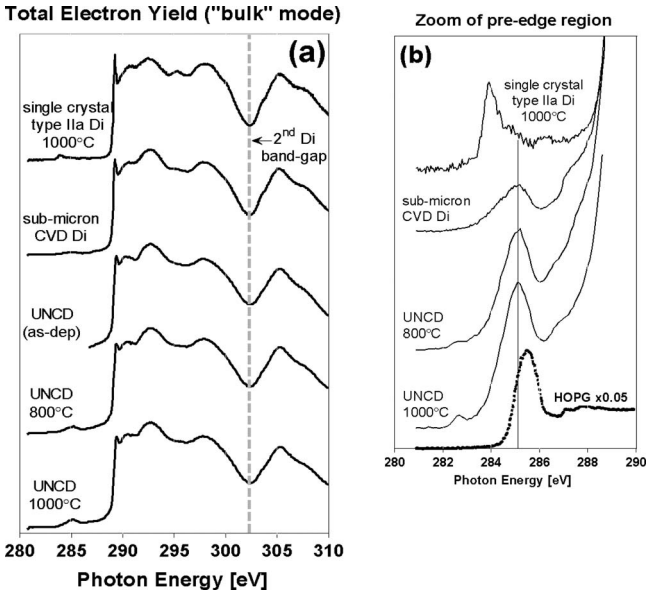

FIG. 1. (a) NEXAFS spectra recorded in the 280–310 eV photon energy range in the TEY mode of single crystal type IIA, microcrystalline CVD diamond film and nanodiamond film following thermal annealing. (b) Zoom of C(1s) core level pre-edge excitation region in the 280–290 eV range. The spectrum of HOPG sample is shown for comparison.

used as a fingerprint of sp^2-coordinated carbon atoms. Analysis and comparison of the graphitic and diamond associated peaks may provide information on the extent of graphitization in each material. Since NEXAFS spectroscopy is equally sensitive to both sp^3 and sp^2 phases of carbon,[47,48] a semiquantitative estimation of the carbon phase composition can be usefully derived from these spectra.

In order to compare the extent of graphitization, peak fitting was performed on the samples that underwent 1000 °C annealing. According to peak fitting analysis the area ratio of the graphitic peak positioned near 284 eV to the area of the diamond second absolute band gap dip[53] positioned near 302 eV is $I_{284}/I_{302}=3.5\%$ for single crystal type IIA diamond sample, while for nanodiamond the same ratio is $I_{284}/I_{302}=5.3\%$ (Fig. 1). These relative graphitization values are much smaller than that derived from NEXAFS analysis of the spectra recorded in surface sensitive mode (see below). In addition, comparing the spectra of as-deposited, 800 and 1000 °C annealed nanodiamond, no drastic change in the line shape or area is observed. It is assumed that in the case of single crystal diamond sample the only possible graphitization channel is the reconstruction of the film surface (i.e., film/vacuum region). Therefore, the observed 3.5% graphitization of this sample is due to the contribution of the sp^2 hybridized surface atoms to the TEY NEXAFS spectrum. Consequently we can conclude that the observed graphitization signal of these nanodiamond films comes from the surface area, while the film's bulk remains nearly unaffected by high temperature annealing. Additional confirmation of this hypothesis may come from the Raman analysis discussed below.

In Fig. 2 the Raman spectra of these nanodiamond films are displayed as a function of annealing temperature up to 1200 °C. The spectrum from the as-deposited film is dominated by well known "nanodiamond" features,[22,23] such as the well known D and G peaks at ~1350 and ~1560 cm^{-1}, respectively, and the transpolyacetylene (t-PA) associated vibrations at 1140 and 1480 cm^{-1}, while the diamond's optical phonon line at 1332 cm^{-1} is strongly overlapped by the graphitic D peak.[22,23] The predominant sp^2 carbon character of the spectrum is due to the higher cross section of the scattered light (at the current wavelength) to sp^2 hybridized carbon, which decreases the sensitivity of the Raman technique to diamond sp^3 carbon.[22] Therefore, the Raman spectrum reflects mainly the grain surface and boundary composition, while the presence of diamond phase is associated with the small peak at 1332 cm^{-1}.

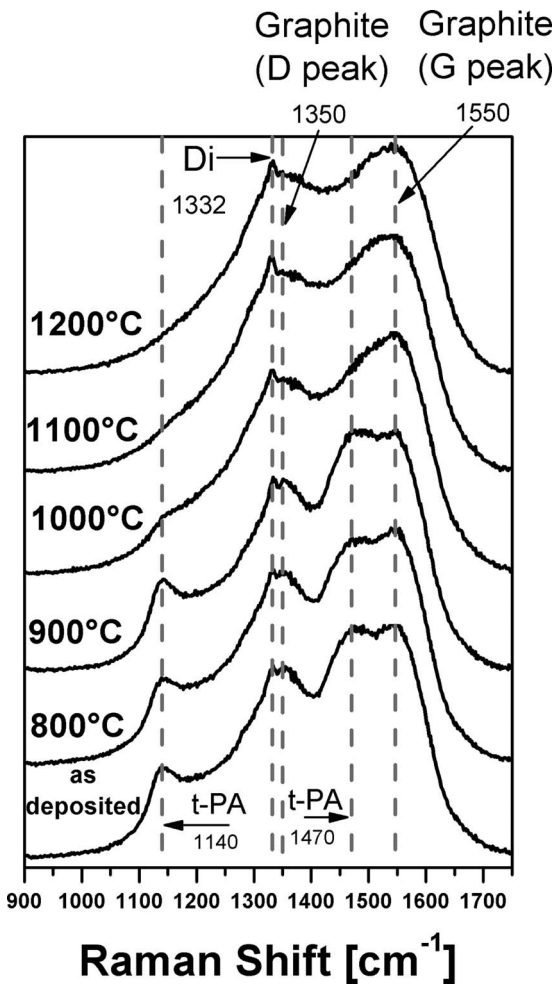

FIG. 2. Raman spectra of nanodiamond diamond films. (a) As-deposited on silicon and following 5×10^{-6} Torr vacuum annealing for 30 min at 800, 900, 1000, 1100, and 1200 °C, as indicated on the plot. Note that t-PA associated peak at 1140 and 1480 cm^{-1} are stable up to 800 °C anneal, decrease in intensity upon 1000 °C anneal, and completely disappear from spectrum under anneal at 1100 °C.

It can be seen from Fig. 2 that the Raman spectra of the nanodiamond film annealed at 800 and 900 °C are similar to that measured for the as-deposited film. However, following annealing at 1000 °C the intensity of t-PA associated features decreases, suggesting thermally enhanced hydrogen (or hydrocarbon) desorption and consequent breaking of t-PA-like bonds. Further annealing at 1100 and 1200 °C results in complete disappearance of t-PA associated peaks, probably indicating bond reconstruction in the film bulk.

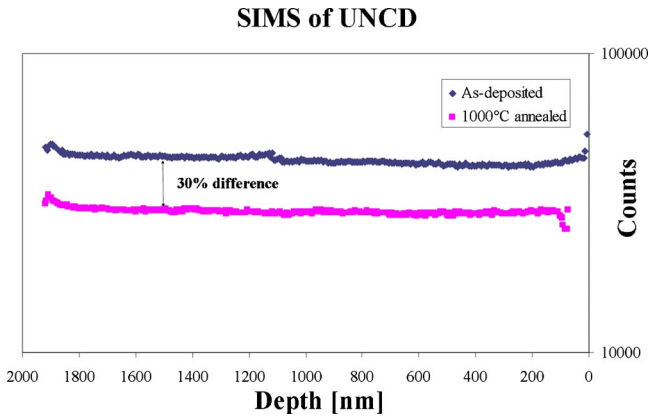

FIG. 3. (Color online) SIMS profile of hydrogen within nanodiamond film. Note the decrease in H concentration from by 30% following 1000 °C annealing.

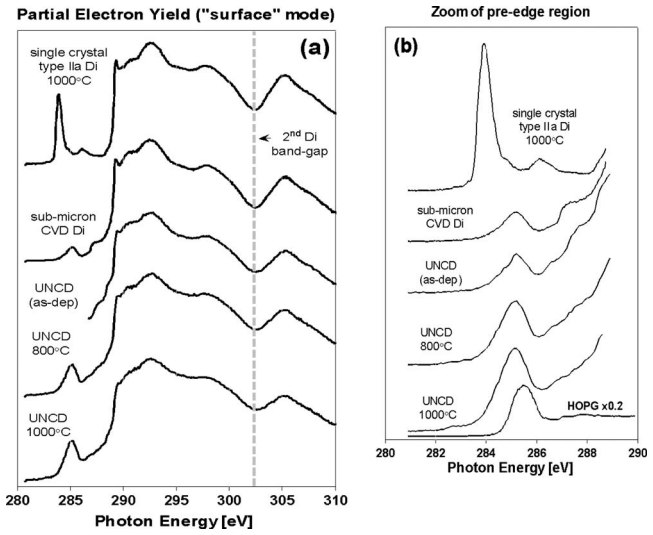

FIG. 4. (a) NEXAFS spectra recorded in the 280–310 eV photon energy range in the PEY mode collecting 8 eV electrons of single crystal type IIA, microcrystalline CVD diamond film and nanodiamond film following thermal annealing. (b) Zoom of C(1s) core level pre-edge excitation region in the 280–290 eV range. The spectrum of HOPG sample is shown for comparison.

A few things may be mentioned regarding this Raman analysis. First, the stability of the diamond phase up to 1200 °C annealing is indicated by the presence of the diamond optical phonon peak at 1332 cm^{-1}. Second, breaking of C—H bonds positioned in grain boundary regions start only at 1000 °C, indicating high thermal stability of hydrogen atoms in the nearest proximity to diamond grains. For comparison, the thermal stability of C—H bonds detected in amorphous carbon does not exceed 600–700 °C.[54–58] Finally and most interesting, it may be observed that breaking C—H bonds of t-PA-like fragments does not change drastically the shape of the Raman spectrum. The unchanging graphitic G peak suggests either a gentle rearrangement of carbon sp^2 bonds in the grain boundary or desorption of entire hydrocarbon species, rather than an increase in graphitic bond production following C—H bond breaking. An estimation of the hydrogen concentration decrease in the films upon annealing to 1000 °C can be derived from SIMS measurements as shown in Fig. 3. It may be concluded that, following annealing at 1000 °C, the concentration of hydrogen atoms decreases by ~30% as compared to the as-deposited film. When compared with the complete removal of the t-PA Raman peak, it must be concluded that either the t-PA bonded hydrogen does not account for the entire hydrogen population within the film, or the t-PA-like bonds partially restructure upon annealing, hence maintaining some hydrogen content in the films above 1000 °C. Obviously higher temperature annealing increases hydrogen loss from the film's bulk. However neither NEXAFS nor Raman analysis provide clear evidence of graphitization of film bulk region. We leave these puzzling results for discussion in Sec. III C.

B. Nanodiamond surface thermal stability study

Surface stability of the nanodiamond films was studied by NEXAFS spectroscopy, recorded in PEY. In addition, we refer to our recent studies of nano- and submicron diamond surface stability investigated by high resolution electron energy loss spectroscopy (HR-EELS),[42] which is ultimately sensitive to the few upper atomic layers.[59]

In Fig. 4 NEXAFS spectra of the same films as in Fig. 1 are shown now recorded in the surface sensitive mode. These spectra are dominated by the same diamond features as before, while the bulk diamond signatures are less pronounced, for example, the contrast of the second absolute diamond band gap at ~302 eV is smaller compared to the surface originated mode at ~284 eV. Comparison of the ratio of these two peak areas reveals $I_{284}/I_{302}=31.6\%$ and $I_{284}/I_{302}=46.6\%$ for single crystal and nanodiamond samples, respectively (Fig. 4). These values are nearly one order of magnitude greater than those derived from bulk sensitive NEXAFS spectra (Fig. 1, Sec. III A). It may be concluded that, similar to single-crystal samples, surface graphitization of nanodiamond films occur at much greater extent than within the film bulk.

We can corroborate these results by looking at recent studies of the thermal stability of fully hydrogenated submicron and nanodiamond film surface by means of HR-EELS.[42] Complete hydrogen loss was detected on both kinds of surfaces under flash annealing at 1000 °C, which results in reconstruction of surface and appearance of C=C dimer features (emerging as HR-EELS peak at ~90 meV energy loss for submicron films). In addition, the extent of graphitization was stronger on the surface of nanodiamond films, in agreement with theoretical predictions of lower thermal stability of nanosized diamond crystallites, compared to submicron ones.[21] However, in that work, no comparison with the film's bulk is shown in terms of the extent of graphitization.

C. Discussion of nanodiamond bulk versus surface thermal stability

Based on the aforementioned analysis of the bulk and surface thermal stability of nanodiamond films the following main experimental conclusions may be listed:

(1) NEXAFS analysis reveals that the diamond *bulk* region is stable up to at least 1000 °C annealing, while accord-

ing to Raman spectroscopy no visible graphitization is observed up to 1200 °C.

(2) SIMS spectroscopy detects loss of ~30% of hydrogen atoms following annealing at 1000 °C, despite a complete loss of the t-PA Raman signature. Importantly this loss of hydrogen atoms is not followed by film bulk graphitization.

(3) Surface analysis by means of NEXAFS reveals nearly full graphitization of the surface area which is confirmed by previous HR-EELS study.[42] Our conductive probe atomic force microscopy measurements (data not shown) confirm this finding detecting ~40% increase in average conductivity and conductivity spikes possibly associated with graphitization of the small grains in the closest vicinity of on the film's surface.

The aforementioned experimental findings may be discussed from the standpoint of the presently accepted nanodiamond stability model[21] together with a few new suggestions.

We start the analysis by considering the lower stability of the film's surface region as compared to the film bulk. This issue may be explained in terms of high energy surface atoms rearrangement and the lack of volume constraint effects on the film's surface. It was previously found that at 927 °C (1200 K) nanocrystalline diamond prepared by a detonation method transforms into bucky diamond,[14] and raising the annealing temperature to 1227 °C (1500 K), led to a cluster with graphitic shells and a diamond core. A high resolution transmission electron microscopy study has shown that graphitization starts from the surface of individual ND crystallites.[60] The widely accepted scenario[21] of nanodiamond thermal reconstruction is that ND graphitization under annealing proceeds from the surface to the bulk and also that edges of exfoliated graphitelike sheets merge with the upper untransformed diamond phase. The presence of surface terminating groups affects the onset temperature of this process: graphitization cannot begin until the surface groups start to decompose.[21] Recently we have shown that graphitization of fully hydrogenated diamond films composed of submicron and nanocrystalline grains starts only following H atom desorption, and similarly proceeds from the surface toward the crystalline bulk.[42] The extent of graphitization is larger in the case of nanodiamond films, which cannot be restored by subsequent *in situ* atomic hydrogen adsorption. In addition, according to the density difference, diamond→graphite transition requires ~30% volume expansion which may be hampered in the film's bulk by tight binding of the crystallite agglomerates.

Now we turn to the analysis of the bulk graphitization of CVD nanodiamond films. Two mutually contradictory experimental results may be seen: the lack of noticeable bulk graphitization up to 1200 °C anneal (Raman, NEXAFS), while visible degradation of t-PA Raman peaks were observed along side with ~30% decrease in bulk hydrogen atom concentration (SIMS).

It has been commonly accepted since 2001 that diamond films prepared by CVD methods contain sp^2 hybridized hydrogenated carbon, which is bonded in a similar way as t-PA molecule within the grain boundary region.[61] Many studies were done to clarify the origin of this bonding by means of isotopic substitution (H/D and $^{12}C/^{13}C$) and thermal annealing.[22–24,40] It was previously observed and reported that upon annealing to elevated temperatures (~1200 °C) the ν_1 and ν_3 peaks associated with C—H bending and C=C stretching vibrations detected at 1140 and 1480 cm^{-1} by Raman spectroscopy are completely removed from the spectrum.[22,23] This is explained by thermal decomposition of t-PA-like bonds at the nanodiamond crystallites grain boundaries. Similar to the present case, no additional change in the spectra shape was detected.[22,23] Since Raman spectroscopy is usually more sensitive to sp^2 carbon phases, some enhancement in G peak intensity may be expected following t-PA bonding decomposition. However, Ferrari and Robertson noted that the rest of the spectrum is substantially unchanged following 1200 °C annealing,[22] while in the work of Pfeiffer *et al.*[62] following 1200 °C annealing the diamond 1332 cm^{-1} line is even more pronounced, than for as-deposited films. Present NEXAFS measurements confirm Raman results revealing at most only minor bulk graphitization of the film.

These findings suggest that during thermal decomposition of the t-PA-like bonds no graphitization occurs within the film bulk, while 30% of hydrogen atoms were lost after the annealing procedure. Therefore, the hydrogen/hydrocarbon atoms produced by thermal decomposition of t-PA seem to play an important role in dynamic stability of nanodiamond grains during annealing. Indeed, studying detonation nanodiamond films by x-ray scattering and diffraction techniques, Aleksenskii *et al.*[63] found that annealing the film in a molecular hydrogen atmosphere for different temperatures increases the relative amount of diamond component within the bulk with a maximum at 800 °C, while the same annealing in Ar atmosphere does not result in this maximum. This effect was attributed to preferential etching of sp^2 carbon atoms by hydrogen as during the CVD process itself.[63] This may be also true in these present results, with the hydrogen atoms being produced by decomposition of hydrocarbons in the grain boundaries, subsequently etching out the loosely bonded sp^2 carbon matrix.

In addition, partial transfer of carbon from the shell to the core with the intermediate formation of hydrocarbon cannot be ruled out. The coalescence of a few grains into single crystal was observed by Aleksenskii *et al.*[63] during annealing in hydrogen, while Lytovich and Banhart[64] directly observed growth of diamond crystallites from graphite phase by electron irradiation. It is well known that up to ~5 nm size nanodiamond particles are energetically preferred over nanographite.[2,3] Moreover, the presence of hydrogen atoms and C—H surface bonding increases the thermodynamic stability range up to ~10 nm (i.e., up to relevant size of the present study).[10] Therefore it is a reasonable suggestion that following C—H bond breaking [bond energy of ~3.5 eV (Ref. 65)] excited carbon atoms may be incorporated into more stable diamond cores, especially in the case of nanodiamond crystallites.

It should be noted finally that the onset for bulk graphitization commonly detected for detonation nanodiamond is

~800 °C,[21] while present results suggest that bulk of the CVD nanodiamond films resists graphitization up to 1200 °C. The difference between these two kinds of materials, among other things, is the composition of intergrain regions; for example, in Raman spectra of detonation films, t-PA features are absent. It may be concluded that hydrogen termination of grain surfaces and the presence of hydrocarbon molecules within the film's grain boundary region intrinsically increases the films' stability against elevated temperatures.

IV. SUMMARY

Relative thermal stability of CVD nanodiamond surface and bulk regions were studied by NEXAFS and Raman spectroscopies. It was found that the surface of the film undergoes nearly complete graphitization at 1000 °C, while the bulk region is stable beyond 1200 °C. This is in contrast with the graphitization onset of ~800 °C reported by other authors for detonation nanodiamond. SIMS analysis showed that annealing at 1000 °C results in a ~30% decrease in the hydrogen concentration, which correlates well with the disappearance of t-PA associated Raman peaks. Notably, breaking of C—H bonds and desorption of H atoms does not result in substantial graphitization of the film's bulk region. The proposed function of hydrogen atoms is a stabilization of diamond grains together with possible preferential etching of nondiamond phase during thermal decomposition of t-PA-like hydrocarbons.

ACKNOWLEDGMENTS

This research project was carried out with the financial support of the Israeli Academy of Science and Arts, the Technion Fund for Promotion of Research, and the Australian Research Council. A.H. was supported as an international research fellow of the Australian Research Council during the project.

[1] G. Davies and T. Evans, Proc. R. Soc. London, Ser. A **328**, 413 (1972).
[2] M. Y. Gamarnik, Phys. Rev. B **54**, 2150 (1996).
[3] M. Y. Gamarnik, Nanostructured Mater. **7**, 651 (1996).
[4] B. B. Pate, Surf. Sci. **165**, 83 (1986).
[5] Yu. V. Butenko, V. L. Kuznetsov, A. L. Chuvilin, V. N. Kolomiichuk, S. V. Stankus, R. A. Khairulin, and B. Segall, J. Appl. Phys. **88**, 4380 (2000).
[6] M. V. Baidakova, V. I. Siklitsky, and A. Ya. Vul, Chaos, Solitons Fractals **10**, 2153 (1999).
[7] S. J. Kwon and J.-G. Park, J. Phys.: Condens. Matter **19**, 386215 (2007).
[8] J. Chen, S. Z. Deng, J. Chen, Z. X. Yu, and N. S. Xua, Appl. Phys. Lett. **74**, 3651 (1999).
[9] A. S. Barnard, S. P. Russo, and I. K. Snook, Phys. Rev. B **68**, 073406 (2003).
[10] A. S. Barnard, Diamond Relat. Mater. **15**, 285 (2006).
[11] G.-D. Lee, C. Z. Wang, J. Yu, E. Yoon, and K. M. Ho, Phys. Rev. Lett. **91**, 265701 (2003).
[12] Z. L. Wang, J. J. Li, Z. H. Sun, Y. L. Li, Q. Luo, C. Z. Gua, and Z. Cui, Appl. Phys. Lett. **90**, 133118 (2007).
[13] C. Liu, X. Xiao, J. Wang, B. Shi, V. Adiga, R. Carpick, J. Carlisle, and O. Auciello, J. Appl. Phys. **102**, 074115 (2007).
[14] J.-Y. Raty, G. Galli, C. Bostedt, T. W. Buuren, and L. J. Terminello, Phys. Rev. Lett. **90**, 037401 (2003).
[15] K. H. Wu, X. R. Wang, S. Liu, and E. G. Wang, J. Appl. Phys. **90**, 4810 (2001).
[16] S. Y. Luo, J. K. Kuo, B. Yeh, J. C. Sung, C. W. Dai, and T. J. Tsai, Mater. Chem. Phys. **72**, 133 (2001).
[17] Y. M. Wong, W. P. Kang, J. L. Davidson, S. Raina, and J. H. Huang, Diamond Relat. Mater. **18**, 563 (2009).
[18] F. A. M. Koeck and R. J. Nemanich, Diamond Relat. Mater. **18**, 232 (2009).
[19] A. Stacey, S. Prawer, S. Rubanov, R. Akhvlediani, Sh. Michaelson, and A. Hoffman, J. Appl. Phys. **106**, 063715 (2009).
[20] F. J. Himpsel, J. A. Knapp, J. A. VanVechten, and D. E. Eastman, Phys. Rev. B **20**, 624 (1979).
[21] V. L. Kuznetzov and Y. V. Butenko, in *Ultra Nanocrystalline Diamond Films: Synthesis, Properties and Applications*, edited by O. A. Shenderova and D. M. Gruen (William Andrew, New York, 2006), p. 405 (and references therein).
[22] A. C. Ferrari and J. Robertson, Philos. Trans. R. Soc. London, Ser. A **362**, 2477 (2004).
[23] H. Kuzmany, R. Pfeiffer, N. Salk, and B. Gunther, Carbon **42**, 911 (2004).
[24] Sh. Michaelson and A. Hoffman, Diamond Relat. Mater. **15**, 486 (2006).
[25] Sh. Michaelson and A. Hoffman, Diamond Relat. Mater. **14**, 470 (2005).
[26] D. Ballutaud, F. Jomard, B. Theys, C. Mer, D. Tromson, and P. Bergonzo, Diamond Relat. Mater. **10**, 405 (2001).
[27] J. Robertson, Diamond Relat. Mater. **3**, 361 (1994).
[28] Y. Lifshitz, Th. Köhler, Th. Frauenheim, I. Guzmann, A. Hoffman, R. Q. Zhang, X. T. Zhou, and S. T. Lee, Science **297**, 1531 (2002).
[29] Y. Lifshitz, X. Meng, S. Lee, R. Akhveldiany, and A. Hoffman, Phys. Rev. Lett. **93**, 056101 (2004).
[30] C. R. S. da Silva, J. F. Justo, and A. Fazzio, Phys. Rev. B **65**, 104108 (2002).
[31] D. F. Talbot-Ponsonby, M. E. Newton, J. M. Baker, G. A. Scarsbrook, R. S. Sussmann, A. J. Whitehead, and S. Pfenninger, Phys. Rev. B **57**, 2264 (1998).
[32] V. Ralchenko, A. Khomich, R. Khmelnitskii, A. Vlasov, and P. N. Lebedev, in *Hydrogen Materials Science and Chemistry of Metal Hydrides*, edited by T. N. Veziroğlu, S. Yu. Zaginaichenko, D. V. Schur, and V. I. Trefilov (Kluwer Academic, New York, 2002), Vol. 82, pp. 203–212.
[33] P. Reichart, G. Datzmann, A. Hauptner, R. Hertenberger, C. Wild, and G. Dollinger, Science **306**, 1537 (2004).
[34] C. J. Tang, M. A. Neto, M. J. Soares, A. J. S. Fernandes, A. J. Neves, and J. Grácio, Thin Solid Films **515**, 3539 (2007).
[35] D. Ballutaud, F. Jomard, T. Kociniewski, E. Rzepka, H. Girard, and S. Saada, Diamond Relat. Mater. **17**, 451 (2008).
[36] S. A. Rakha, C. Jianqing, X. Huihao, Y. Guojun, D. Zhu, and J. Gong, Diamond Relat. Mater. **18**, 1247 (2009).
[37] D. Ballutaud, T. Kociniewski, J. Vigneron, N. Simon, and H. Girard, Diamond Relat. Mater. **17**, 1127 (2008).
[38] Sh. Michaelson, O. Ternyak, R. Akhvlediani, A. Hoffman, A. Lafosse, R. Azria, O. A. Williams, and D. M. Gruen, J. Appl. Phys. **102**, 113516 (2007).
[39] Sh. Michaelson, O. Ternyak, A. Hoffman, and Y. Lifshitz, Appl. Phys. Lett. **90**, 031914 (2007).
[40] Sh. Michaelson, O. Ternyak, R. Akhvlediani, and A. Hoffman, J. Chem. Vap. Deposition **14**, 196 (2008).
[41] Sh. Michaelson and A. Hoffman, Diamond Relat. Mater. **17**, 920 (2008).
[42] Sh. Michaelson, R. Akhvlediani, and A. Hoffman, J. Appl. Phys. **104**, 083527 (2008).
[43] J. F. Morar, F. J. Himpsel, G. Hollinger, G. Hughes, and J. L. Jordan, Phys. Rev. Lett. **54**, 1960 (1985).
[44] G. Comelli, J. Storh, C. J. Robinson, and W. Jark, Phys. Rev. B **38**, 7511 (1988).
[45] J. F. Morar, F. J. Himpsel, G. Hollinger, J. L. Jordon, G. Hughes, and F. R. McFelly, Phys. Rev. B **33**, 1346 (1986).
[46] J. F. Morar, F. J. Himpsel, G. Hollinger, G. Hughes, and F. R. McFeely, Phys. Rev. B **33**, 1340 (1986).
[47] F. L. Coffman, R. Cao, P. A. Pianetta, S. Kapoor, M. Kelly, and L. J. Terminello, Appl. Phys. Lett. **69**, 568 (1996).
[48] A. Heiman, I. Gouzman, G. Comtet, L. Hellner, G. Dujardin, S. Christiansen, H. Strunk, and A. Hoffman, J. Appl. Phys. **89**, 2622 (2001).
[49] D. Zhou, D. M. Gruen, L. C. Qin, T. G. McCauley, and A. R. Krauss, J. Appl. Phys. **84**, 1981 (1998).
[50] D. Zhou, T. G. McCauley, L. C. Qin, A. R. Krauss, and D. M. Gruen, J. Appl. Phys. **83**, 540 (1998).
[51] O. Ternyak, A. A. Cimmino, S. Prawer, and A. Hoffman, Diamond Relat. Mater. **14**, 272 (2005).
[52] Australian synchrotron website, http://www.synchrotron.org.au/.
[53] The area of the second absolute diamond band gap dip was calculated in the following way: the background line was defined between two local

maxima at 297 and 305 eV and module of the obtained dip area was calculated by means of usual software.
[54]M. Benlahsen, B. Racine, K. Zellama, and G. Turban, J. Non-Cryst. Solids **283**, 47 (2001).
[55]Ch. Wild and P. Koidl, Appl. Phys. Lett. **51**, 1506 (1987).
[56]J. K. Walters, D. M. Fox, T. M. Burke, O. D. Weedon, R. J. Newport, and W. S. Howells, J. Chem. Phys. **101**, 4288 (1994).
[57]J. K. Walters, J. S. Rigden, R. J. Newport, S. F. Parker, and W. S. Howells, Phys. Scr., T **T57**, 142 (1995).
[58]M. Lejeune, M. Benlahsen, and R. Bouzerar, Appl. Phys. Lett. **84**, 344 (2004).
[59]H. Ibach and D. L. Mills, *Electron Energy Loss Spectroscopy and Surface Vibrations* (Academic, New York, 1982).
[60]V. L. Kuznetsov, A. L. Chuvilin, Y. V. Butenko, I. L. Malkov, and V. M. Titov, Chem. Phys. Lett. **222**, 343 (1994).
[61]A. C. Ferrari and J. Robertson, Phys. Rev. B **63**, 121405 (2001).
[62]R. Pfeiffer, H. Kuzmany, P. Knoll, S. Bokova, N. Salk, and B. Gunther, Diamond Relat. Mater. **12**, 268 (2003).
[63]A. E. Aleksenskii, M. V. Baidakova, A. Ya. Vul', A. T. Dideikin, V. I. Siklitskii, and S. P. Vul', Phys. Solid State **42**, 1575 (2000).
[64]Y. Lyutovich and F. Banhart, Appl. Phys. Lett. **74**, 659 (1999).
[65]D. deB. Darwent, *Bond Dissociation Energies in Simple Molecules* (National Bureau of Standards, Washington, 1970).